Polymer 50 (2009) 534–540

Contents lists available at ScienceDirect

Polymer

journal homepage: www.elsevier.com/locate/polymer

Hydration behavior of perfluorinated and hydrocarbon-type proton exchange membranes: Relationship between morphology and proton conduction

Naohiko Takimoto [a,*], Libin Wu [a], Akihiro Ohira [a,*], Yuko Takeoka [a,b], Masahiro Rikukawa [b]

[a] Polymer Electrolyte Fuel Cell Cutting-edge Research Center (FC-Cubic), National Institute of AIST, 2-41-6 Aomi, Koto-ku, Tokyo 135-0064, Japan
[b] Department of Materials and Life Science Engineering, Sophia University, 7-1 Kioi-cho, Chiyoda-ku, Tokyo 102-8554, Japan

ARTICLE INFO

Article history:
Received 13 June 2008
Received in revised form
6 November 2008
Accepted 14 November 2008
Available online 28 November 2008

Keywords:
Proton exchange membrane
Small-angle X-ray scattering
Atomic force microscopy

ABSTRACT

The relationships between morphology and proton conduction for Nafion membranes and hydrocarbon-type proton exchange membranes, namely, sulfonated poly(arylene ether ether ketone) (S-PEEK) and sulfonated poly(arylene ether sulfone) (S-PES), were investigated by small-angle X-ray scattering (SAXS) and atomic force microscopy (AFM). The direct simultaneous observation of surface morphology and active regions of proton conduction on membranes by combined high-resolution AFM phase imaging and an electrochemical technique at controlled humidity provided significant morphological information, particularly for the hydrocarbon-type membranes that exhibit few or no features on SAXS profiles. For the Nafion membranes, the active proton paths became denser and congregated with each other at over 60% RH, resulting in the formation of well-connected networks. For the hydrocarbon-type membranes, however, only the relatively small and dispersed proton paths were observed, which showed no significant change even as water content increased. We have demonstrated that the differences in microscopic morphology between the Nafion and hydrocarbon-type membranes are associated with the differences between their macroscopic proton conductivities.

1. Introduction

Fuel cells have attracted much attention as promising alternative power generators owing to their advantages of high energy efficiency, noiseless operation, and environmental friendliness as compared to present energy sources. Among the various types of fuel cells, the proton exchange membrane fuel cells (PEMFCs) have been anticipated to become available for many applications, such as power sources for vehicles, residential co-generations, and portable electronic devices [1].

Proton exchange membranes (PEMs), which are one of the most important components of PEMFCs, have various characteristic requirements: high proton conductivity at lower humidity; a high gas barrier; and high mechanical and chemical stabilities. A number of polymer electrolyte materials such as perfluorinated and hydrocarbon ionomers have been developed among the various types of PEMs. Perfluorosulfonic acid/polytetrafluoroethylene copolymers (PFSA) such as Nafion, Aciplex, and Flemion are state-of-the-art materials because of their high mechanical, thermal and chemical stabilities as well as their high proton conductivity [2–7]. Hydrocarbon (HC)-type membranes have extensively been studied from the viewpoints of cost, environmental friendliness, and stability at high temperatures [8,9].

With the developments in polymer synthesis, deeper understanding of the structural properties for polymer electrolytes is now a prime issue in the development of high-performance membranes, as well as in the elucidation of the relationship between the morphology and physical properties (e.g., proton conductivity, gas permeability, and chemical and physical stabilities) of polymer electrolytes [10,11]. For PFSA-type membranes, much knowledge of their surface and bulk morphologies has been accumulated by structural observation methods such as AFM and transmission electron microscopy (TEM), and by structure analysis methods such as SAXS, small-angle neutron scattering (SANS), wide-angle X-ray diffraction (WAXD) analysis, and nuclear magnetic resonance (NMR) [3]. The scattering and diffraction methods such as SAXS, SANS and WAXD analysis are powerful tools for analyzing bulk morphology [3,12–22]. Thus, numerous scattering and diffraction studies based on various morphological models involving specific assumptions on the structure of Nafion have been reported, and the morphological information has led to a reconsideration of the detailed relationships among the

* Corresponding authors. Tel.: +81 0 3599 8553; fax: +81 3 3599 8554.
E-mail addresses: nao-takimoto@aist.go.jp (N. Takimoto), a-oohira@aist.go.jp (A. Ohira), m-rikuka@sophia.ac.jp (M. Rikukawa).

0032-3861/$ – see front matter © 2008 Elsevier Ltd. All rights reserved.
doi:10.1016/j.polymer.2008.11.029

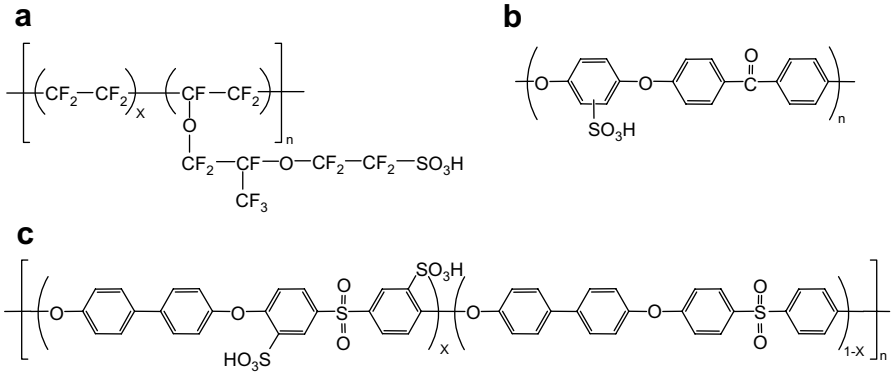

Fig. 1. Chemical structures of (a) Nafion, (b) S-PEEK, and (c) S-PES.

morphology, proton conductivity, and gas permeability of membranes [3,12,23–27]. On the other hand, there is less morphological information on HC-type membranes than on Nafion, because most of them show few or no features in their scattering and diffraction profiles. Therefore, for HC-type membranes, direct observation methods under ordinary and/or humidified conditions are more promising for obtaining morphological information than indirect observation methods described above.

AFM enables the direct visualization under various environmental conditions such as temperature and humidity, so some unique and interesting AFM studies of Nafion membranes have been reported [16–18,28–32]. Recently, a direct imaging of active proton-conductive regions using conductive AFM based on current detection (current image), which is normally conducted in the contact mode coupled with an electrochemical technique, has also been reported [28–30]. Furthermore, we first succeeded in the simultaneous observation of the proton conduction and surface morphology of Nafion using not the contact mode but the phase mode coupled with an electrochemical technique [31]. The direct simultaneous imaging clearly revealed that phase images have higher correlation with current images than topographic images. In HC-type membranes, however, the observation of morphological alternation during humidity changes still remains rare because it is difficult to identify hydrophilic regions by only the conventional AFM-AC mode owing to the absence of any ordered structures or the presence of very few ones that can be observed in detail. As mentioned above, although direct observation using the AC mode is a powerful tool, further improvements in the direct observation of hydrophilic regions are still desired, particularly for HC-type membranes.

Here, we report the hydration behavior of Nafion membranes and HC-type membranes, namely, sulfonated poly(ether ether ketone) (S-PEEK) and random copolymer types of biphenol-based sulfonated poly(arylene ether sulfone) (S-PES) [33,34] (Fig. 1). We determine the proton conductivities and structural properties of the membranes using SAXS and AFM in the phase mode, coupled with an electrochemical method under precisely controlled temperature and humidity. Although the HC-type membranes exhibit a relatively high proton conductivity at a high humidity (e.g., 90% RH), their proton conductivity is considerably lower than that of Nafion membranes at a low humidity (e.g., 50% RH). This difference seems to be due to the differences in morphological property between the membranes related to their proton-conductive area. We discuss the relationship between the morphology and proton conduction of membranes determined through the analysis of their bulk structure by SAXS and the direct visualization of active proton path by AFM under precisely controlled humidity.

2. Experimental section

2.1. Membrane preparation

As PFSA-type membranes, several commercially available Nafion membranes namely, N-115 (1100 equivalent weight (EW), 127 μm thickness, acid form) and N-117 (1100 EW, 178 μm thickness, acid form), were purchased from DuPont and used as-received.

HC-type polymers were synthesized as described in the literature. S-PEEK was synthesized by the sulfonation of a commercial PEEK polymer with concentrated sulfuric acid [35]. S-PES was synthesized by direct aromatic nucleophilic substitution polycondensation [33,34]. The HC-type polymers were cast from *N*-methyl-2-pyrrolidone (NMP) solutions onto a glass substrate and dried at 80 °C under vacuum. The membranes were immersed in 0.5 M sulfuric acid overnight for complete protonation, then rinsed with deionized water and dried under ambient condition. Their thicknesses were 60 μm (S-PEEK) and 50 μm (S-PES), and their ion exchange capacities (IECs) were 1.87 meq/g (S-PEEK) and 1.60 meq/g (S-PES), respectively, as determined by back titration.

2.2. Water uptake and proton conductivity

Water uptake and proton conductivity were measured using an isothermal absorption measurement system (MSB-AD-V-FC, BEL Japan Inc.) equipped with an impedance analyzer (Solartron SI 1260). This system enabled the simultaneous measurements of water uptake and proton conductivity in the same chamber. Each

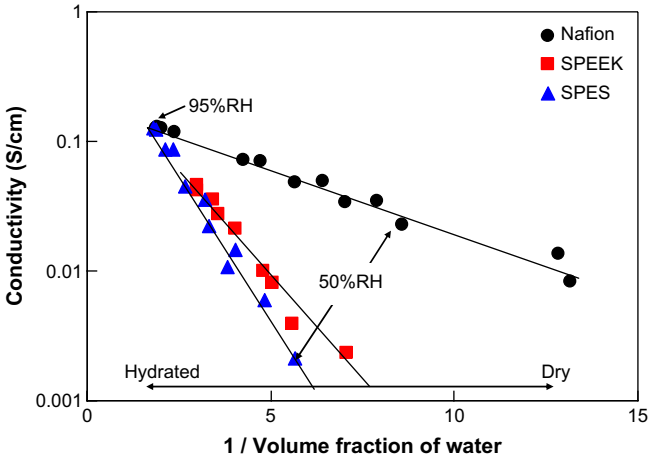

Fig. 2. Proton conductivity of Nafion N-117, S-PEEK, and S-PES membranes as a function of volume fraction of water at 40 °C.

membrane sample was dried at 80 °C for 1 h under dry nitrogen flow, then exposed to a humidified nitrogen environment at 40 °C. After there was no further weight change of each sample, sample weight and proton conductivity were measured sequentially. Humidity conditions were changed stepwise from 10% RH to 95% RH.

The water uptake of membranes was calculated as

$$\text{Water volume fraction } (\mathrm{Vf}_{\mathrm{H_2O}}) = \left(W_{\mathrm{wet}} - W_{\mathrm{dry}}\right)/d_{\mathrm{H_2O}}/V_{\mathrm{dry}}$$

where W_{wet} and W_{dry} are the weights of wet and dry membranes, respectively. V_{dry} is the volume of dry membranes, and $d_{\mathrm{H_2O}}$ is the value of water density (1 g/cm^3).

Proton conductivity was measured using a four-point probe cell. The AC impedance spectrum was recorded over the frequency range from 10 Hz to 100 kHz using an impedance analyzer. Proton conductivity was calculated from dry membrane thickness and membrane resistance was taken at the frequency that produced the minimum imaginary response.

2.3. SAXS

SAXS was performed using a high-power X-ray system (Rigaku Corporation, Nano-Viewer) with three optical slits, a confocal Max Flux mirror, and an X-ray generator of Cu Kα radiation ($\lambda = 1.542$ Å). The scattered X-ray intensity was recorded with a 2D flat camera. The samples were set in a sealed chamber equipped with temperature and humidity sensors. A wet-gas generator was connected to adjust the humidity in the chamber. Temperature was controlled by the water cryostat. All samples were sealed in a certain condition for at least 1 h before measurements. The distance between a sample and the camera was 500–550 mm in length. All data were corrected for background (dark current) and plotted as a function of the magnitude of the scattering vector q defined as $q = (4\pi/\lambda)\sin\theta$ with λ being the wavelength, and 2θ being the scattering angle.

2.4. AFM and current-mapping image

AC-mode AFM and current-mapping images were obtained using a JSPM-5400 (Nihon Denshi) with a humidity control unit [31]. A Pt-coated cantilever (TAP-300E, Budgetsensors) with a force constant of 40 N/m and a resonance frequency of 300 kHz was used. Membrane samples were placed on a gold-plated conductive sample stage with Nafion dispersion (DE-2020, DuPont) as adhesives. Before AFM observations, a sample was placed in a humidity controlled chamber for at least 1 h. Bias voltage was applied to the sample stage during observations. All the topography, phase, and current-mapping images were simultaneously obtained.

3. Results and discussion

3.1. Water uptake and proton conductivity

The results of water uptake and proton conductivity measurements of Nafion, S-PEEK, and S-PES membranes at 40 °C (Fig. 2) clearly show a difference in the hydration–conduction relationship between the PFSA- and HC-type membranes: the PFSA- and the HC-type membranes differ in the effect of water content on proton conductivity. In Fig. 2, the slope of proton conductivity against the water uptake for Nafion is much lower than that for S-PEEK and S-PES. This means that the dependence of proton conductivity on the water content is much stronger for the HC-type membranes than that for the PFSA-type membranes, and this stronger dependence reflects poor conductivity of HC-type membranes at lower RH. At 95% RH, where membranes are almost fully hydrated, Nafion and S-PES have similar water contents ($1/\mathrm{Vf}_{\mathrm{H_2O}} = 2$) and proton conductivities (ca. 0.1 S/cm). As humidity decreases to 50% RH, the proton conductivities of S-PES and Nafion decrease to 0.001 S/cm and 0.02 S/cm, respectively, even though much water content remains for S-PES membranes. S-PEEK shows nearly the same hydration–conduction relationship as S-PES. These results reveal that the proton conductivity of HC-type membranes is easily lowered with a decrement of water content, even if the proton conductivity is as high as that of PFSA-type membranes at high humidity. This significant difference in the hydration–conduction relationship is thought to be caused by structural factors such as connectivity, width, and other morphologies of the "active" proton paths that pass through the membrane [36].

3.2. Changes in bulk morphologies studied by SAXS

To investigate the changes in bulk morphologies of the membrane samples during hydration, SAXS was performed at 20–80% RH. The SAXS curves of N-117 exhibited scattering maxima at q close to 0.32–0.41 nm^{-1} at all relative humidities, which were

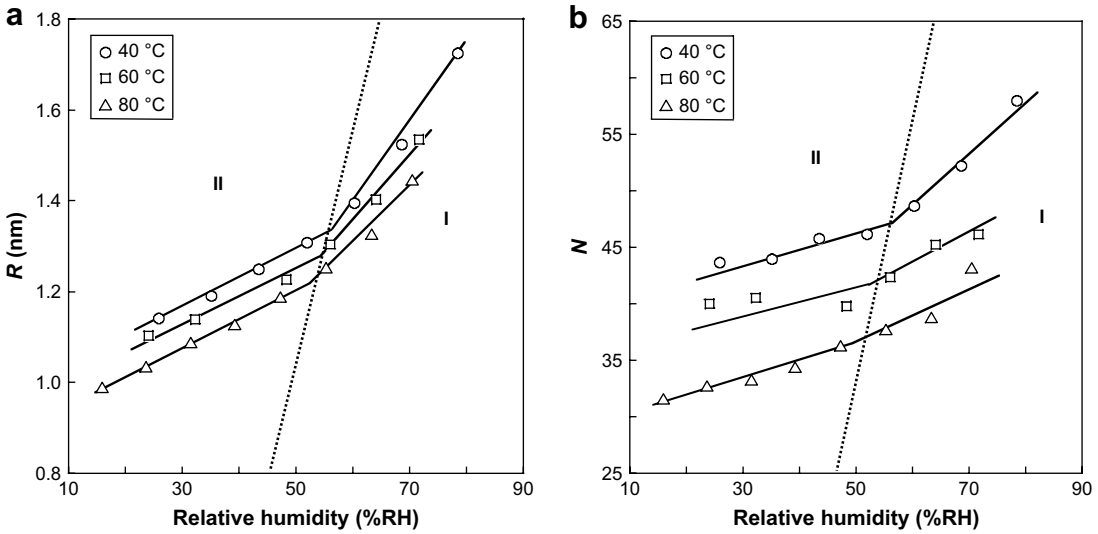

Fig. 3. Humidity dependencies of (a) the size of hydrophilic domains, R, and (b) the number of ionic groups in one hydrophilic domain, N, for Nafion N-117 at various temperatures.

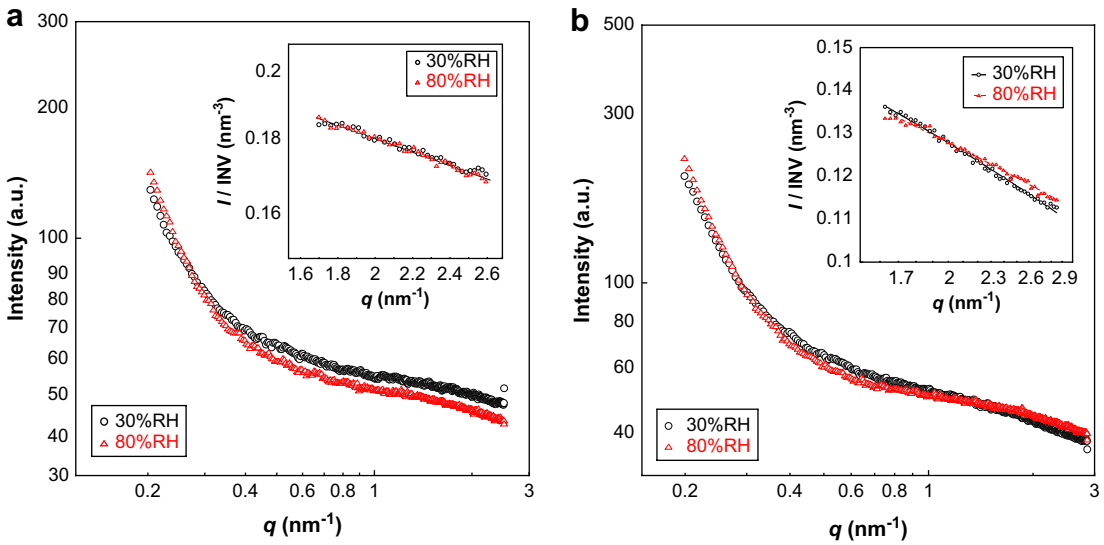

Fig. 4. SAXS profiles of (a) S-PEEK and (b) S-PES at 40 °C at various humidities. The insets show the intensity normalized by the scattering invariant (INV) vs. scattering vector (q). The scattering invariant for two system is defined as INV $= \int_0^q I(q)q^2dq$.

attributed to hydrophobic domains. Furthermore, the other scattering maxima were observed at $q = 1.1$–2.9 nm^{-1} at higher relative humidities and were attributed to hydrophilic domains in Nafion, as reported by several researchers [22].

The effect of humidity (water uptake) on hydrophilic domains is illustrated more clearly by the changes in the radius of hydrophilic domains, R, and the number of ionic groups in one hydrophilic domain, N, calculated based on the cluster-channel model which is the most widely known structure model of Nafion [37]. Fig. 3 shows the humidity dependencies of R and N for Nafion N-117 at 40, 60, and 80 °C. In Fig. 3, both R and N increase with relative humidity and change more sharply above 50–60% RH (area I), compared with the values at lower RH% region (area II). It is clear that the hydration behaviors in these two areas are different. For area II, each hydrophilic domain (ionic cluster) expands gradually with water absorption, and there is less congregating behavior among hydrophilic domains. In contrast, for area I, several small hydrophilic domains rearrange into larger domains, and more ionic groups congregate into larger hydrophilic domains. This behavior is similar to that in the temperature range examined in this study, despite a notable temperature effect. In particular, the humidity dependency in area I is more distinct at lower temperatures. The hydrophilic domains become smaller with an increase in temperature at the same relative humidity. Moreover, the inflection points for R and N shift to lower humidity at higher temperature. This shift is due to the accelerated mobility of ionic side chains at higher temperatures [38]. From these results, further hydrophilic/hydrophobic phase separation in the amorphous phase may be induced in Nafion with water adsorption, and this assumption could be derived if any other structure models are applied [12,15,16].

Nanoscale bulk structures in the two HC-type membranes are significantly different from those in the PFSA-type membranes. No distinct scattering peaks such as those observed in Nafion could be observed in S-PEEK and S-PES at 30–80% RH, as shown in Fig. 4. Despite the lack of scattering peaks from hydrophilic domains, scattering intensity values decreased at $q > 1.6$ nm^{-1} for S-PEEK and at $q > 1.8$ nm^{-1} for S-PES (insets in Fig. 4). This is due to the existence of a hydrophilic/hydrophobic internal interface [36]. The slopes of these decreasing intensity curves are almost independent of humidity. This reflects that the internal interface hardly changes even at high humidity. The SAXS profiles indicate that nanoscale phase separation is less pronounced and the distribution of water is more homogeneous in S-PEEK and S-PES than that in Nafion.

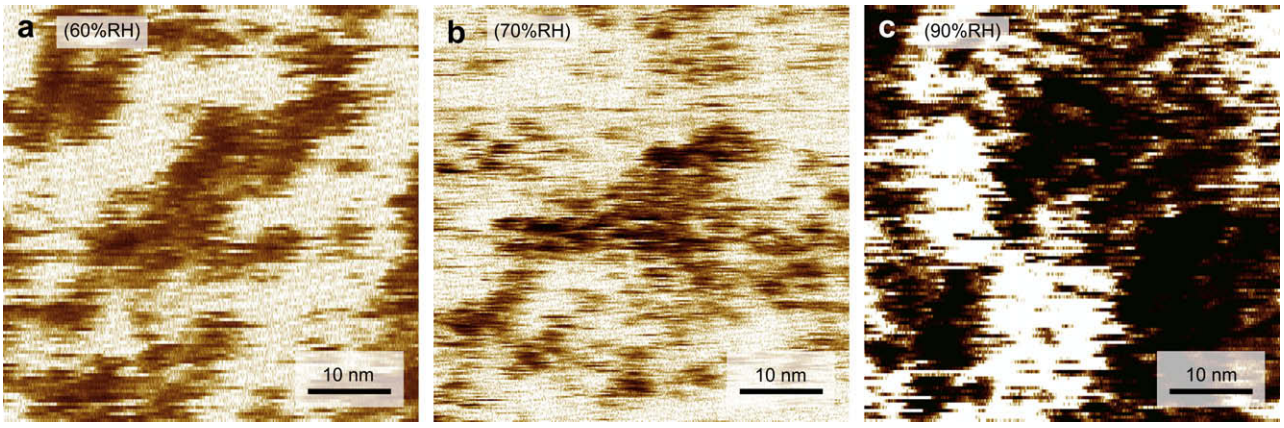

Fig. 5. AC-AFM current-mapping images of Nafion N-115 over a range of humidity of 60–90% RH. z-Scale maximum: 5 pA. Scan size: 50 nm × 50 nm. Scan rate: 5 Hz. Applied bias voltage: −1.5 V.

3.3. Direct visualization of proton path rearrangement for PFSA

Fig. 5 depicts AC-AFM current-mapping images of the Nafion membrane obtained at various relative humidities. These images clearly show changes in proton-conductive regions during hydration conditions. At 60% RH (Fig. 5a), dark areas in the image corresponding to proton-conductive regions appear blurred and no pronounced spots are observed. When relative humidity increases to 70% (Fig. 5b), many darker spots, however, become distinguishable, and these grow in size with increasing humidity and congregate into a larger area (Fig. 5c). This phenomenon can be interpreted as the rearrangement of hydrophilic regions. The rearrangement of proton-conductive regions is observed over 70% RH in the current-mapping images obtained at 22 °C. This is in good agreement with the SAXS results, indicating that the rearrangement begins from higher RH at lower temperature. At lower RH, the conductive paths are not well defined and many small ionic clusters are dispersed in hydrophilic-rich amorphous regions; therefore, sorbed water is also delocalized in such amorphous regions to form large conductive networks. When the ionic clusters grow in size with increasing water content, they combine with each other and form effectively connected conductive paths. Thus, the rearrangement observed in the current-mapping images is thought to involve further hydrophilic/hydrophobic phase separation of the amorphous regions.

3.4. Active proton paths of HC-type membranes

Fig. 6 depicts the simultaneously obtained AC-AFM phase images and current-mapping images of S-PEEK (A and a) and S-PES (B and b) at 22 °C and 90% RH. Images of Nafion N-115 membranes are also presented for comparison (C and c). Fig. 6a–c shows remarkable differences between the PFSA- and HC-type membranes. The most notable difference is the distribution of dark areas corresponding to proton-conductive regions in the current-mapping images: the proton-conductive regions of HC-type membranes are much more distributed over the surface and much more isolated from each other compared with those of the PFSA-type membranes. For Nafion (Fig. 6c), the proton-conductive or non-proton-conductive regions are clearly separated, and proton-conductive regions are congregated, thereby forming large (>10 nm) active areas. On the other hand, the proton-conductive regions show poor congregation into active areas, and the proton-conductive or non-proton-conductive regions are not well separated for the HC-type membranes (Fig. 6a and b). In particular, the conductive spots of S-PES seem to be small compared with those for the Nafion membranes, while the non-proton-conductive grains covering the surface (bright areas) appear to be small. These features reveal that each active proton path in the HC-type membranes is narrow, which may be caused by its poorly developed hydrophilic/hydrophobic phase separation, as mentioned in the previous section.

The correlations between surface morphology and proton-conductive regions are also noteworthy. The proton-conductive regions for Nafion (Fig. 6A and a) are observed in exactly the same positions as the dark areas in the phase images, which correspond to hydrophilic regions. In contrast, for the HC-type membranes (Fig. 6A and a for S-PEEK, and Fig. 6B and b for S-PES), poor correlations between the phase image and the current-mapping image were observed. The proton-conductive regions of the HC-type membranes are sometimes observed in bright areas of their phase images, which have been interpreted as hydrophobic regions. These results reveal that phase images do not necessarily correlate to the active proton paths of the HC-type membrane surface, in contrast to the previous understanding of phase images [33,34]. There are two possible explanations for this phenomenon. One is that the dark areas in phase images do not necessarily correspond to hydrophilic regions. For non-crystalline polymers,

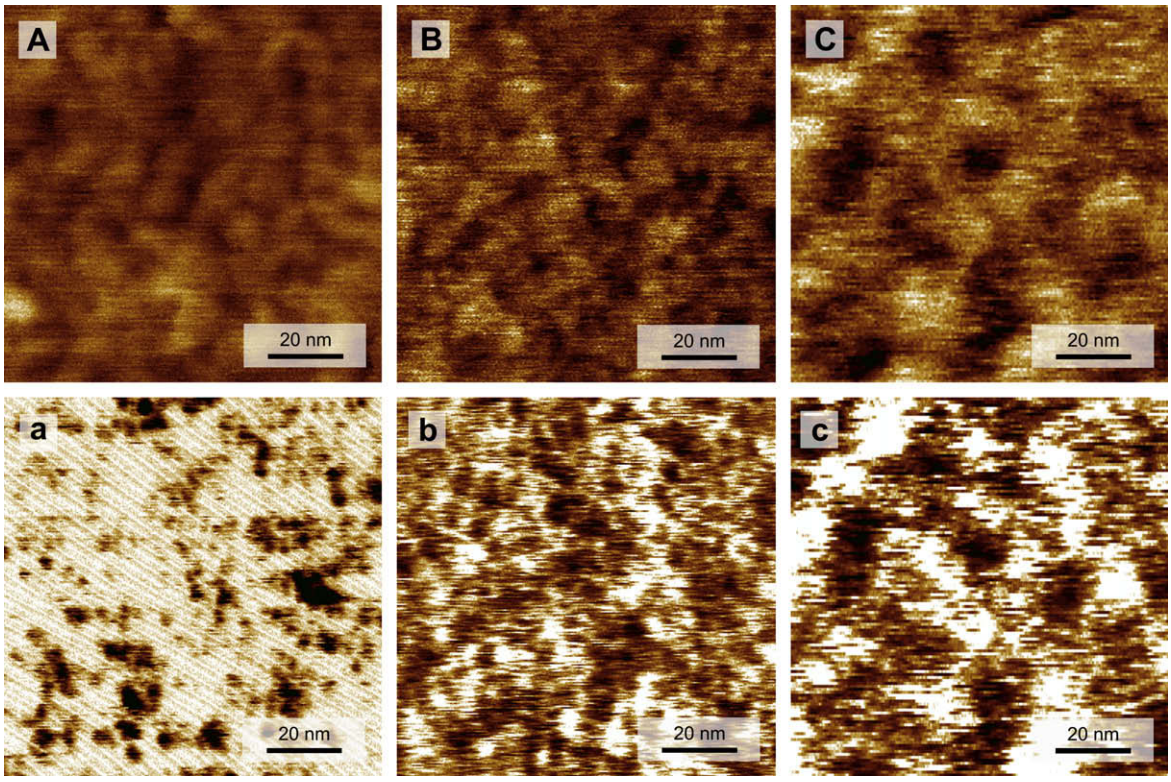

Fig. 6. AC-AFM images of (A, a) S-PEEK, (B, b) S-PES, and (C, c) Nafion N-115 at 90% RH. (A)–(C) are phase images (*z*-scale 20°), and (a)–(c) are corresponding current-mapping images (*z*-scale maximum 10 pA). Scan size is 100 nm × 100 nm. Scan rate: 5 Hz. Applied bias voltage: −1.5 V.

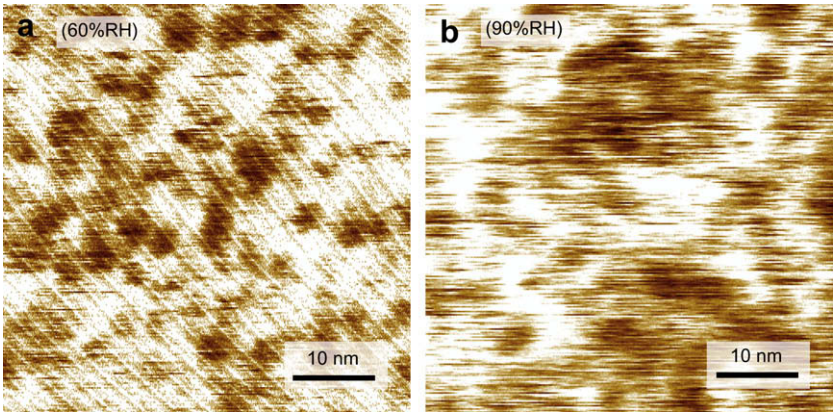

Fig. 7. AC-AFM current-mapping images of S-PES at (a) 60 and (b) 90% RH. *z*-Scale maximum: 3 pA (a) and 9 pA (b). Scan size is 50 nm × 50 nm. Scan rate: 5 Hz. Applied bias voltage: −1.5 V.

particularly, it is difficult to correlate all the features of phase images correctly; thus, much more careful consideration is necessary for the interpretation of phase images. The other explanation is that not all hydrophilic regions are "active", even if the contrast of phase images reflects the hydrophilicity/hydrophobicity of the membrane surface. This means that there must be many "dead-end" paths, an incomplete network caused by the lack of water or a poor phase separation of the polymer; however, none of these can be distinguished in the phase images. Therefore, the main advantage of this AFM current-mapping method is that not only surface morphology but also connectivity of the proton paths through the inside of the membrane can be observed.

The effect of relative humidity on proton-conductive areas is also examined. The HC-type membranes showed no clear evidence of the morphological changes such as phase separation, rearrangement, or coagulation of the proton path during hydration. The current-mapping images of S-PES obtained at 60% RH (Fig. 7a) and 90% RH (Fig. 7b) indicated no significant changes of the proton-conductive regions, which were observed as small dispersed spots under all the conditions, while the number of spots and the current value of each spot increased with increasing RH. This result reveals that the hydrophilic/hydrophobic phase separation in the HC-type membranes poorly develops with hydration, a conclusion which is also supported by the results of bulk structural investigations.

These differences in hydration behavior related to morphological changes are a key to explain the difference in the RH dependence of proton conductivity between the PFSA- and HC-type membranes. For the PFSA-type membranes, the presence of rearrangement suggests that the hydrophilic regions are relatively flexible, that is, it is easy to change the shape and size of domains by changing RH. This feature enables the connections of network of conductive paths to be maintained even if the water content decreases. Well-developed hydrophilic/hydrophobic phase separation is also important. Sorbed water in PFSA-type membranes is delocalized in the hydrophilic domains; thus, the water volume fraction in the hydrophilic domains is higher than that in the bulk membrane.

On the other hand, for the HC-type membranes, the absence of rearrangement prevents the optimization of proton paths (e.g., path shrinkage and localization of absorbed water); thus, the networks are easily disconnected with decreasing water content. This absence of rearrangement in the HC-type membranes is ascribable to the relatively rigid backbones and the entanglement of polymer chains that confer higher mechanical properties to the membrane. Particularly, in the aromatic type system in which hydrophilic groups are directly attached to the backbone, the main chains seem not to be flexible enough to allow hydrophilic groups to induce hydrophilic/hydrophobic phase separation during solvent evaporation in the casting process. Once constructed, hydrophilic domains are difficult to rearrange for optimal proton conduction.

4. Conclusions

The hydration behavior related to the proton conduction and morphological changes of PFSA- and HC-type PEMs were investigated by SAXS and AFM. The PFSA-type membranes showed well-developed hydrophilic/hydrophobic phase-separated structures both on their surfaces and in bulk. Active proton paths were found to congregate into large proton-conductive regions in the PFSA-type membranes. In addition, our results suggest the rearrangement of hydrophilic regions during hydration. This interesting behavior of the PFSA-type membranes seems to be the key to the high proton conductivity at low RH. For the HC-type membranes, however, only relatively small and dispersed proton paths were observed, which show no significant change even with an increase in water content. Moreover, a very poor relationship between the phase image and the current-mapping image was observed for the HC-type membranes. This poor relationship indicates that a very careful interpretation of typical AFM images is necessary in determining surface morphology.

Our results also suggest that well-designed microscopic morphologies, which can connect the proton path with a small amount of sorbed water, are necessary to improve proton conductivity at low RH. For example, block-copolymer-type membranes with nanophase separation of hydrophilic/hydrophobic domains are promising, if the polymer design and casting process controlling phase separation can be established [39]. Thus, our observation technique, which can directly visualize an active proton path, will be a powerful tool for characterizing proton-conducting polymer electrolytes.

Acknowledgements

This work was supported by the Ministry of Economy, Trade and Industry, Japan.

References

[1] Vielstich W, Lamm A, Gasteiger H. Handbook of fuel cells: fundamentals, technology, and applications. Hoboken, NJ: Wiley; 2003.
[2] Souzy R, Ameduri B. Prog Polym Sci 2005;30:644–87.
[3] Mauritz KA, Moore RB. Chem Rev 2004;104:4535–85.
[4] Banerjee S, Curtin DE. J Fluorine Chem 2004;125:1211–6.
[5] Arcella V, Troglia C, Ghielmi A. Ind Eng Chem Res 2005;44:7646–51.
[6] Yoshida N, Ishisaki T, Watakabe A, Yoshitake M. Electrochim Acta 1998;43:3749–54.
[7] Wakizoe M, Velev OA, Srinivasan S. Electrochim Acta 1995;40:335–44.

[8] Rikukawa M, Sanui K. Prog Polym Sci 2000;25:1463–502.
[9] Hickner MA, Ghassemi H, Kim YS, Einsla BR, McGrath JE. Chem Rev 2004;104:4587–612.
[10] Yang Y, Holdcroft S. Fuel Cells 2005;5:171–86.
[11] Kreuer KD, Paddison SJ, Spohr E, Schuster M. Chem Rev 2004;104:4637–78.
[12] Schmidt-rohr K, Chen QS. Nat Mater 2008;7:75–83.
[13] Osborn SJ, Hassan MK, Divoux GM, Rhoades DW, Mauritz KA, Moore RB. Macromolecules 2007;40:3886–90.
[14] Chen QS, Schmidt-rohr K. Macromol Chem Phys 2007;208:2189–203.
[15] Kim MH, Glinka CJ, Grot SA, Grot WG. Macromolecules 2006;39:4775–87.
[16] Rubatat L, Gebel G, Diat O. Macromolecules 2004;37:7772–83.
[17] Umemura K, Wang T, Hara M, Kuroda R, Uchida O, Nagai M. Langmuir 2006;22:3306–12.
[18] James PJ, Antognozzi M, Tamayo J, McMaster TJ, Newton JM, Miles MJ. Langmuir 2001;17:349–60.
[19] James PJ, McMaster TJ, Newton JM, Miles MJ. Polymer 2000;41:4223–31.
[20] Lehmani A, Durand-Vidal S, Turq P. J Appl Polym Sci 1998;68:503–8.
[21] Porat Z, Fryer JR, Huxham M, Rubinstein I. J Phys Chem 1995;99:4667–71.
[22] Fujimura M, Hashimoto T, Kawai H. Macromolecules 1981;14:1309–15.
[23] Hickner MA, Pivovar BS. Fuel Cells 2005;5:213–29.
[24] Affoune AM, Yamada A, Umeda M. J Power Sources 2005;148:9–17.
[25] Lee K, Ishihara A, Mitsushima S, Kamiya N, Ota K. J Electrochem Soc 2004;151:A639–45.
[26] Gode P, Lindbergh G, Sundholm G. J Electroanal Chem 2002;518:115–22.
[27] Broka K, Ekdunge P. J Appl Electrochem 1997;27:117–23.
[28] Aleksandrova E, Hiesgen R, Friedrich KA, Roduner E. Phys Chem Chem Phys 2007;9:2735–43.
[29] Bussian DA, O'Dea JR, Metiu H, Buratto SK. Nano Lett 2007;7:227–32.
[30] Xie X, Kwon O, Zhu D-M, Nguyen TV, Lin G. J Phys Chem B 2007;111:6134–40.
[31] Takimoto N, Ohira A, Takeoka Y, Rikukawa M. Chem Lett 2008;37:164–5.
[32] McLean RS, Doyle M, Sauer BB. Macromolecules 2000;33:6541–50.
[33] Wang F, Hickner M, Ji Q, Harrison W, Mecham J, Zawodzinski TA, et al. Macromol Symp 2001;175:387–95.
[34] Wang F, Hickner M, Kim YS, Zawodzinski TA, McGrath JE. J Membr Sci 2002;197:231–42.
[35] Kobayashi T, Rikukawa M, Sanui K, Ogata N. Solid State Ionics 1998;106:219–25.
[36] Kreuer KD. J Membr Sci 2001;185:29–39.
[37] Gierke TD, Munn GE, Wilson FC. J Polym Sci Polym Phys Ed 1981;19:1687–704.
[38] Bauer F, Denneler S, Willert-Porada M. J Polym Sci Part B Polym Phys 2005;43:786–95.
[39] Ghassemi H, Ndip G, McGrath JE. Polymer 2004;45:5855–62.